Supporting Information

Carr et al. 10.1073/pnas.1718917115

SI Materials and Methods

Absorption and Emission Characterization. An aqueous solution of ICG (Pfaltz & Bauer), IRDye 800CW PEG (LI-COR Biosciences), or IR-E1050 (Nirmidas Biotech) was prepared in quartz cuvettes. Absorption spectra were recorded on a Cary 5000 UV-Vis-NIR IR spectrometer (Varian). To collect the emission spectra, samples were excited with a 635-nm diode laser (Thorlabs), and emission was collected using a pair of off-axis parabolic mirrors and directed to a single-grating spectrometer (Spectra Pro-300i; Acton). An InGaAs-calibrated photodiode (DET10N; Thorlabs) was used to detect the intensity of the emission. As the determination of the spectral responsivity is critical to accurately measuring the fluorescence spectrum of ICG, we calibrated the fluorescence setup across the visible-, NIR-, and SWIR-wavelength ranges. Using a 200 W Quartz Tungsten Halogen Lamp (Newport Instruments), we acquired a spectrum that we compared with the known spectral irradiance of the lamp to arrive at a spectral responsivity curve as depicted in Fig. S1*C*. We further corrected the fluorescence spectra for solvent reabsorption as described in our previous work (1). For plots in energy, we also applied the Jacobian correction. The effects of these corrections on the raw spectrum are provided in Fig. S1*D*. The emission spectrum of ICG was also measured using excitation from a 532-nm diode laser, and the resulting emission was detected on a silicon-based spectrometer (QE65000; OceanOptics).

The ICG tail emission was further characterized using an InGaAs camera. The emission intensity of ICG in water (0.027 mg/mL) was measured in 20-nm spectral bands across the SWIR using an InGaAs SWIR camera (Princeton Instruments NIRvana 640). A glass vial containing the ICG solution was illuminated with 50–70 mW/cm^2 of light from a 10-W 808-nm laser (MLL-N-808; Opto Engine) coupled to a 910-μm core metal-cladded multimode fiber (MHP910L02; Thorlabs) and diffused through a ground glass plate (DG10-220-MD; Thorlabs). The peak emission of the laser was measured to be 809 nm. The emitted light was directed from the imaging stage to the camera using a 4-inch square first surface silver mirror (part no. 84448; Edmund Optics), filtered through two colored glass 850-nm long-pass filters (FGL850S; Thorlabs) and through a liquid crystal tunable filter (VariSpec LNIR; 20-nm bandwidth; PerkinElmer), and focused onto the SWIR camera with a C-mount objective (SWIR-35; Navitar). The tunable filter was scanned from 900 to 1,650 nm in 25-nm steps. A final image at 950 nm was acquired to ensure that the intensity matched the first measurement, verifying that the ICG solution was not bleached throughout the measurement.

Photoluminescence Quantum Yield. Quantum yield measurements were obtained using an integrating sphere (RTC-060-SF; Labsphere). The sample was illuminated using a 785-nm diode laser with an excitation power of 25 mW that was modulated at 260 Hz. The output was collected using a calibrated germanium detector (Newport: 818-IR) through a Stanford Research Systems lock-in amplifying system. Colored glass long-pass filters (2× Schott Glass RG800 or 1× RG850) were used to block the excitation beam. The sample was placed in a polytetrafluoroethylene (PTFE)-capped quartz cuvette, and a solvent blank was used to ensure a consistent environment inside the integrating sphere. The measured photocurrent was adjusted to account for the external quantum efficiency of the detector when calculating the quantum yield. Finally, the measured quantum yield was corrected to account for leakage of the excitation light and the transmittance of the filter. Additional quantum yield justification is given below.

While measuring the absolute quantum yield of IR-E1050 using an integrating sphere, we found a lower value (0.2%) compared with the one reported by the manufacturer (2%), which used the dye IR-26 as reference for relative quantum yield measurements. These relative quantum yield measurements relied on a quantum yield of 0.5% for IR-26 that was reported by Drexhage and coworkers (2) in 1982. More recently, however, two independent publications by Beard and coworkers (3) (0.05%) and Resch-Genger and coworkers (4) (0.07%) have found the original value to be approximately 10 times too large. Measuring the absolute quantum yield of IR-26 in our laboratory yielded a value of 0.05%, which is in line with these more recent publications. We, therefore, believe that 0.05% is the correct value of the quantum yield of IR-26.

Brightness Comparison of ICG and IR-E1050 in Bovine Blood and Water and in Vivo. To compare emission brightness in blood, ICG, IR-E1050, and IRDye 800CW PEG (LI-COR Biosciences) were diluted in bovine blood (sodium citrate conjugated; Rockland Immunochemicals) to a concentration of 0.01 mg/mL. The solutions were imaged individually and side by side, in the above-described setup with 808-nm excitation, and the emission was filtered through either two colored glass 1,000-nm long-pass filters or through an additional dielectric 1,300-nm long-pass filter. In the resulting background-corrected images, the average emission intensity was calculated from a region of interest within the vials and normalized to the integration time.

To compare the brightness in aqueous solutions, ICG (Pfaltz & Bauer) and IR-E1050 (Nirmidas Biotech) were diluted to a concentration of 0.01 mg/mL in cell culture-grade water and 1× PBS, respectively. The solutions were imaged individually and side by side in the imaging setup with 808-nm excitation, and the emission was filtered through two colored glass 1,000-nm long-pass filters and an additional dielectric 1,300-nm long-pass filter. In the resulting background-corrected images, the average emission intensity was calculated from a region of interest within the vials and normalized to the integration time.

To compare the brightness of the two SWIR emitters in vivo ($n = 2$), ICG and IR-E1050 were injected at the recommended concentrations (ICG: 0.25 mg/mL ~ 322 nmol/mL in cell culture-grade water; IR-E1050: 1 mg/mL ~ 333 nmol/mL in 1× PBS), which yielded a roughly equimolar concentration of both emitters. Two hundred microliters of the respective solution (64 nmol of ICG, 66 nmol of IR-E1050) was injected into the tail vain of an NU/NU nude mouse (12 wk old, male; Taconic Biosciences) within 5–6 s and excited with diffuse 808-nm excitation (50 mW/cm^2). The fluorescence was collected with a commercial SWIR lens (35 mm; Navitar), filtered through two colored glass 1,000-nm long-pass filters, and collected using an InGaAs camera (NIRvana 640; cooled to −80 °C; Princeton Instruments) using an integration time of 1 ms. To estimate the in vivo brightness, the intensity in the heart was measured 1 min postinjection (100-frame average). The results are summarized in Fig. S2 and Movie S1.

Tissue Phantom Imaging. Tissue phantom images (Fig. S3) were taken by submerging a capillary filled with 0.0175 mg/mL aqueous ICG (Pfaltz & Baur) in 20% Intralipid (Baxter Healthcare Corporation) that was diluted to 2% Intralipid in water. Images

were taken in the NIR and the SWIR of the capillary before and after being submerged 3 mm below the surface of the 2% Intralipid solution in the imaging setup described above.

In Vivo Imaging. Noninvasive brain vasculature imaging was performed in two C3H/HeJ mice (21.7 and 20.5 g, female, 10 wk old; The Jackson Laboratory). Mice were anesthetized, and the hair on the head was removed. Mice were injected via the tail vein with up to 200 μL of a 0.025 mg/mL aqueous solution of ICG and immediately imaged using a pair of achromatic doublet lenses [75- and 150-mm effective focal length (EFL), 25.4 mm, C coated; Thorlabs]. Gaussian fitting was performed in MATLAB using the Curve Fitting toolbox.

Heart angiography was performed in three Friend Virus B NIH Jackson mice (male, 18 wk old; The Jackson Laboratory). Mice were anesthetized, and surgery was performed to expose the heart [as for perfusion (5)]. One or two 200-μL boluses of 0.25 mg/mL ICG in water were injected via the tail vein while concurrently imaging the emission. The objective used was composed of a pair of 200-mm focal-length biconvex lenses (25.4 mm, C coated; Thorlabs) and three translatable 500-mm focal-length biconvex lenses (50.8 mm, C coated; Thorlabs) to set the focus.

Intravital brain imaging (Fig. S4) was performed in an NU/NU nude mouse (female, 15 wk old; Massachusetts General Hospital Cox-7 gnotobiotic animal facility) with implanted cranial window. The window was implanted as previously described (6, 7). ICG phospholipids were prepared by dissolving 4.8 mg ICG in a 2:1 mixture of chloroform and methanol, agitating with 23 mg PEG 2000 phospholipids in chloroform (1,2-dioleoyl-*sn*-glycero-3-phosphoethanolamine-*N*-[methoxy(polyethylene glycol)-2000]; ammonium salt; 880130C; Avanti Polar Lipids), drying off the solvent under nitrogen flow, and resuspending the dried phospholipids in 2 mL cell culture-grade water, resulting in a final concentration of 13.9 mg/mL ICG phospholipid solution or 2.4 mg/mL concentration of ICG. The aqueous ICG phospholipid mixture was passed through a 0.22-μm syringe filter before injecting ∼50 μL via the tail vein into the anesthetized mouse, and the fluorescence was immediately imaged. The cranial window of the mouse was fixed to the stage of a Nikon Ti-E inverted microscope equipped with a Stage UP Kit (Nikon) and a backport adaptor, to which an 808-nm laser diode coupled to a fiber was attached. To eliminate laser speckle, we used an Optotune speckle remover (88–397; Edmund Optics). We used a dichroic long-pass filter (DMLP900R for SWIR; Thorlabs; 69–906 for NIR; Edmund Optics) to direct the excitation light to the sample. Imaging was done with a 2× (Nikon CFI Plan Apo Lambda) or a 4× (Nikon CFI Plan Apo Lambda) objective with additional 1.5× magnification from the microscope.

For noninvasive ICG hepatobiliary clearance imaging, an NCr nude mouse (male, 14 wk old; Taconic Biosciences) was anesthetized, placed in the imaging setup with a pair of achromatic doublet lenses (75- and 500-mm EFL, 25.4 mm, C coated; Thorlabs), and injected via a tail vein catheter with 200 μL of ICG at a concentration of 0.25 mg/mL in water. Hepatobiliary clearance of the ICG was then monitored and imaged through intact skin over ∼2 h using an 850-nm dielectric long-pass filter and a silicon detector or an additional 1,200- or 1,500-nm long-pass filter with InGaAs detection. Images shown in Fig. S6*A* and Movie S3 were taken ∼1.5–2 h after the initial ICG injection.

Noninvasive lymph node imaging (Fig. S6*B*) was performed in four C57BL/6 mice (male, 12–15 wk old; The Jackson Laboratory). The mice were anesthetized, the hair was removed, and 10–100 μL of 0.18 mg/mL aqueous solution of ICG was injected s.c. in the left and right hind feet and s.c. in the tail of the mouse. The fluorescence from the dorsal lymph vessels and nodes was immediately imaged through the intact skin using a commercial Navitar lens with 850-, 1,000-, 1,200-, 1,300-, and 1,400-nm long-pass dielectric filters (Thorlabs) and with the biconvex lens system described above.

In Vivo Targeted Imaging with IRDye 800CW. Two tumor-bearing (BT474-Gluc) NU/NU nude mice were prepared using the following procedures. Human HER2-amplified breast cancer BT474 cells were transduced with an expression cassette encoding Gluc and GFP separated by an internal ribosomal entry site using a lentiviral vector as previously described (BT474-Gluc cells) (8). BT474-Gluc cells were maintained in RPMI 1640 supplemented with 10% (vol/vol) FBS (Atlanta Biologicals).

Female nude mice (8–9 wk of age) were implanted with a 0.36- or 0.72-mg 17b-estradiol pellet (Innovative Research of America) the day before implantation of tumor cells. Injection of BT474-Gluc cells in the brain parenchyma was performed as previously described (7, 9, 10). Briefly, the head of the mouse was fixed with a stereotactic apparatus, and the skull was exposed via skin incision. Using a high-speed air-turbine drill (CH4201S; Champion Dental Products) with a burr tip size of 0.5 mm in diameter, three sides of a square (∼2.5 mm in length each side) were drilled through the skull over the left hemisphere of the brain until a bone flap became loose. The bone flap was pulled back, exposing the brain parenchyma; 100,000 BT474-Gluc cells diluted in 1 μL PBS were stereotactically injected into the left frontal lobe of the mouse brain using an insulin syringe. Subsequently, the bone flap was placed back into position in the skull and sealed using histocompatible cyanoacrylate glue, and the skin atop the skull was sutured closed. All animal procedures were performed according to the guidelines of the Public Health Service Policy on Human Care of Laboratory Animals and in accordance with a protocol approved by the Institutional Animal Care and Use Committee of Massachusetts General Hospital.

Tumor growth was determined by measuring the Gluc activity in the blood as previously described (9, 10). Blood Gluc activity was measured with a Promega Glomax 96 microplate luminometer (Fisher Scientific). The correlation between Gluc activity and tumor size was previously determined and established using in vivo ultrasonography imaging performed through a cranial window (9, 10). At the time of imaging, we estimate the tumors to have a size of 50–70 mm^3.

IRDye 800CW was conjugated to trastuzumab (Genentech) (9) using a labeling kit (P/N 928–38040; Li-Cor). Briefly, 1 mg of trastuzumab was dissolved in 900 μL PBS buffer and 100 μL 1 M potassium phosphate buffer (pH 9) to obtain a solution with a pH of 8.5. Twenty-five microliters of ultrapure water was added to the NHS-IRDye 800CW, and the solution was shaken for 2 min until the dye completely dissolved. Eight microliters of the resulting solution were added to the trastuzumab solution, and the mixture was incubated for 2 h at room temperature protected from light. Subsequently, the trastuzumab–dye conjugate was separated from free residual dye using Pierce Zeba desalting spin columns.

Two tumor-bearing (BT474-Gluc) nude mice (9) (female, 11 wk old) were injected i.p. with 330 μL of IRDye 800CW trastuzumab (15-mg/kg dose). Two additional tumor-bearing nude mice were not injected and served as controls. After 3 d, the mice were anesthetized and noninvasively imaged through intact skin and skull using diffuse 808-nm excitation, the previously described pair of achromatic doublet lenses, 850- and 1,000-nm long-pass dielectric filters, and an InGaAs camera (Fig. S7). All mice were then injected via the tail vein with up to 300 μL (3 nmol) of IRDye 800CW PEG (P/N 926–50401; Li-Cor). They were illuminated with 808-nm excitation and imaged with a 850-nm long-pass filter and either a 1,000- or 1,150-nm long-pass filter on an SWIR camera, or they were illuminated with 780-nm excitation (M780L3; Thorlabs) and imaged with an 800-nm long-pass filter on an NIR camera.

1. Cosco ED, et al. (2017) Flavylium polymethine fluorophores for near- and shortwave infrared imaging. *Angew Chem Int Ed Engl* 56:13126–13129.
2. Kopainsky B, Qiu P, Kaiser W, Sens B, Drexhage KH (1982) Lifetime, photostability, and chemical structure of IR heptamethine cyanine dyes absorbing beyond 1 um. *Appl Phys B Photophys Laser Chem* 29:15–18.
3. Semonin OE, et al. (2010) Absolute photoluminescence quantum yields of IR-26 dye, PbS, and PbSe quantum dots. *J Phys Chem Lett* 1:2445–2450.
4. Hatami S, et al. (2015) Absolute photoluminescence quantum yields of IR26 and IR-emissive $Cd_{(1-x)}Hg_{(x)}Te$ and PbS quantum dots–Method- and material-inherent challenges. *Nanoscale* 7:133–143.
5. Gage GJ, Kipke DR, Shain W (2012) Whole animal perfusion fixation for rodents. *J Vis Exp*, 10.3791/3564.
6. Brown E, Munn LL, Fukumura D, Jain RK (2010) In vivo imaging of tumors. *Cold Spring Harb Protoc* 2010:pdb.prot5452.
7. Kodack DP, et al. (2012) Combined targeting of HER2 and VEGFR2 for effective treatment of HER2-amplified breast cancer brain metastases. *Proc Natl Acad Sci USA* 109:E3119–E3127.
8. Chung E, et al. (2009) Secreted Gaussia luciferase as a biomarker for monitoring tumor progression and treatment response of systemic metastases. *PLoS One* 4:e8316.
9. Askoxylakis V, et al. (2015) Preclinical efficacy of ado-trastuzumab emtansine in the brain microenvironment. *J Natl Cancer Inst* 108:djv313.
10. Kodack DP, et al. (2017) The brain microenvironment mediates resistance in luminal breast cancer to PI3K inhibition through HER3 activation. *Sci Transl Med* 9: eaal4682.

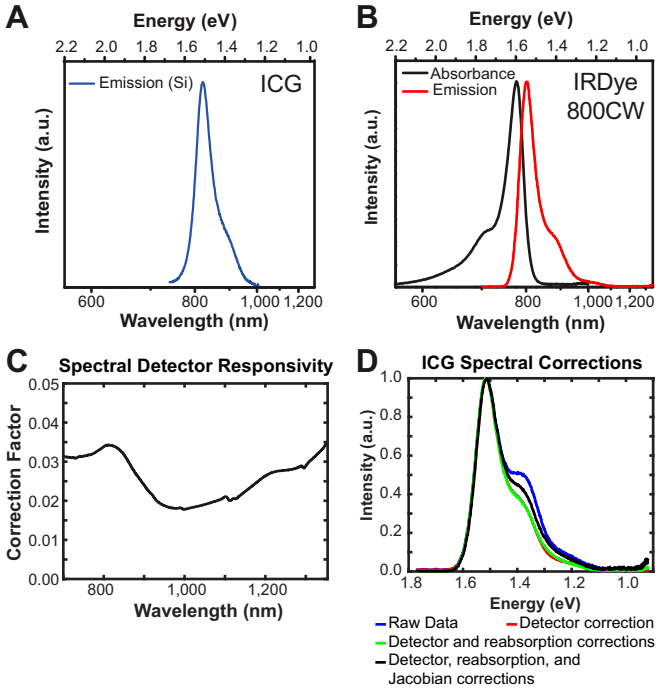

Fig. S1. Optical properties of ICG, IRDye 800CW PEG, and relevant spectral corrections. (*A*) Measuring the emission of ICG using a commercial silicon detector-based spectrometer (QE65000 spectrometer; OceanOptics) artificially truncates the low-energy shoulder of the emission. This emission tail can be recovered with appropriate detection and calibration as shown in Fig. 1. (*B*) We also show here the absorption and emission spectra of aqueous IRDye 800CW PEG. The absorption spectrum (black) exhibits a peak at 776 nm, with a higher-energy shoulder extending into visible wavelengths. The emission spectrum (red), measured using an InGaAs detector-based spectrometer, mirrors the absorption spectrum, exhibiting an emission peak at 801 nm and a lower-energy shoulder extending into SWIR wavelengths. The raw fluorescence spectra of NIR dyes measured using the InGaAs detector-based spectrometer were corrected for the spectral responsivity of the entire spectrometer system (*C*) as well as for solvent reabsorption. For plots depicted on an energy scale, we also applied the Jacobian correction. The effects of all three corrections on the raw spectrum (here exemplified with ICG) are visualized in *D*.

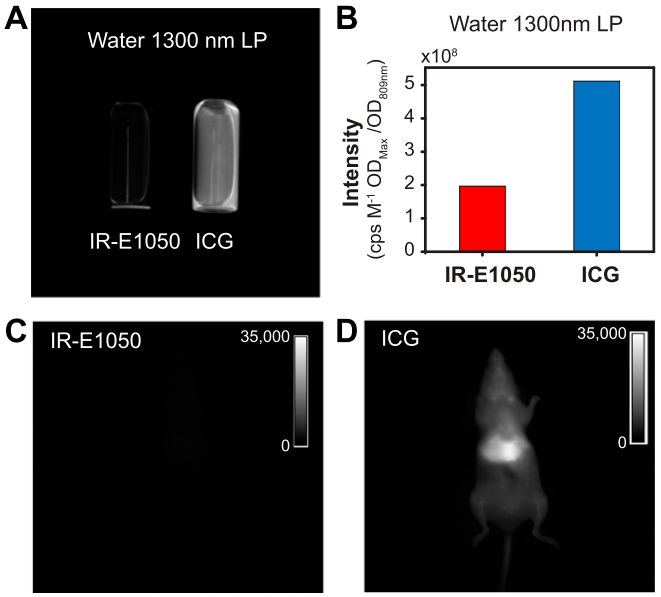

Fig. S2. Comparison of the optical properties of ICG with other NIR and SWIR dyes in water and in vivo. (*A*) We compared the fluorescence intensity of 0.01 mg/mL aqueous solutions of IR-E1050 and ICG on an InGaAs camera with 808-nm excitation. (*B*) The results show superior emission of ICG compared with IR-E1050 from 1,300 to 1,620 nm (1,300-nm LP). SDs for signal intensity were found to be less than 15% for measuring signal intensity in water. Similarly, we found that the in vivo fluorescence intensity of the recommended bolus of (*C*) IR-E1050 (67 nmol) and (*D*) ICG (64 nmol) injected via the tail vein of a mouse was approximately one order of magnitude greater for ICG beyond 1,000 nm. Shown here is the relative fluorescence intensity in the vasculature and in the liver imaged noninvasively through intact skin ~1 min after dye injection.

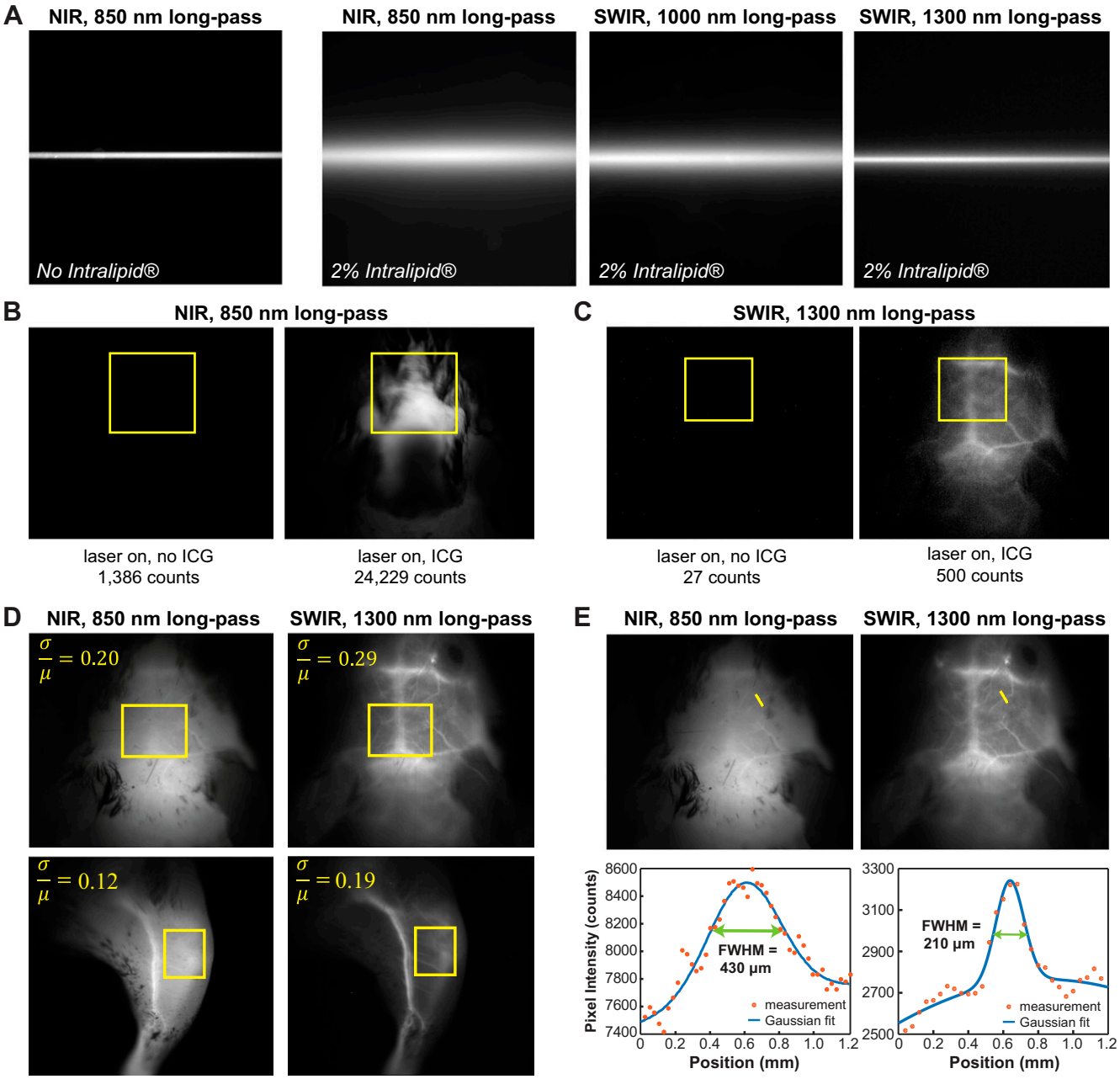

Fig. S3. Control images and contrast quantification of brain and hind-limb vasculature in a mouse. (*A*) A 0.8- to 1.1-mm-wide (i.d.) capillary was filled with aqueous ICG, and the fluorescence was imaged using 850-nm long-pass NIR detection. The capillary was then submerged in ∼3 mm of 2% Intralipid liquid tissue phantom and imaged again with 850-nm long-pass NIR detection, 1,000-nm long-pass SWIR detection, and 1,300-nm long-pass SWIR detection, showing that the scatter of light caused by the tissue phantom is suppressed with increasing imaging wavelength. (*B–E*) Two hundred microliters of aqueous ICG (0.025 mg/mL) was injected into the tail vein of two mice, and the fluorescent vasculature was imaged noninvasively through intact skin. (*B*) The first mouse was imaged before and after ICG injection with 850-nm long-pass NIR detection. Comparing the two images, we see that the scattering of ICG signal is caused by the tissue, and the poor contrast is not attributed to leak through of 808-nm excitation light being imaged on the NIR camera. (*C*) Similarly, there is minimal leak through of excitation light imaged on the SWIR camera using a 1,300-nm long-pass filter, and the majority of detectable signal comes from ICG after being injected. (*D*) The contrast, defined as the SD (σ) divided by the mean (μ) pixel intensity, was quantified to compare NIR and SWIR imaging of the brain vasculature and hind-limb vasculature of a mouse. The contrast was found to be 0.20 for NIR-imaged brain vasculature and 0.29 for SWIR-imaged brain vasculature. The contrasts were 0.12 and 0.19 for NIR- and SWIR-imaged hind-limb vasculature, respectively. (*E*) Apparent vessel width was also calculated by finding the FWHM of a two-term Gaussian fit to the intensity profile of a brain vessel. The apparent vessel widths wer 430 and 210 μm for NIR- and SWIR-imaged brain vasculature, respectively.

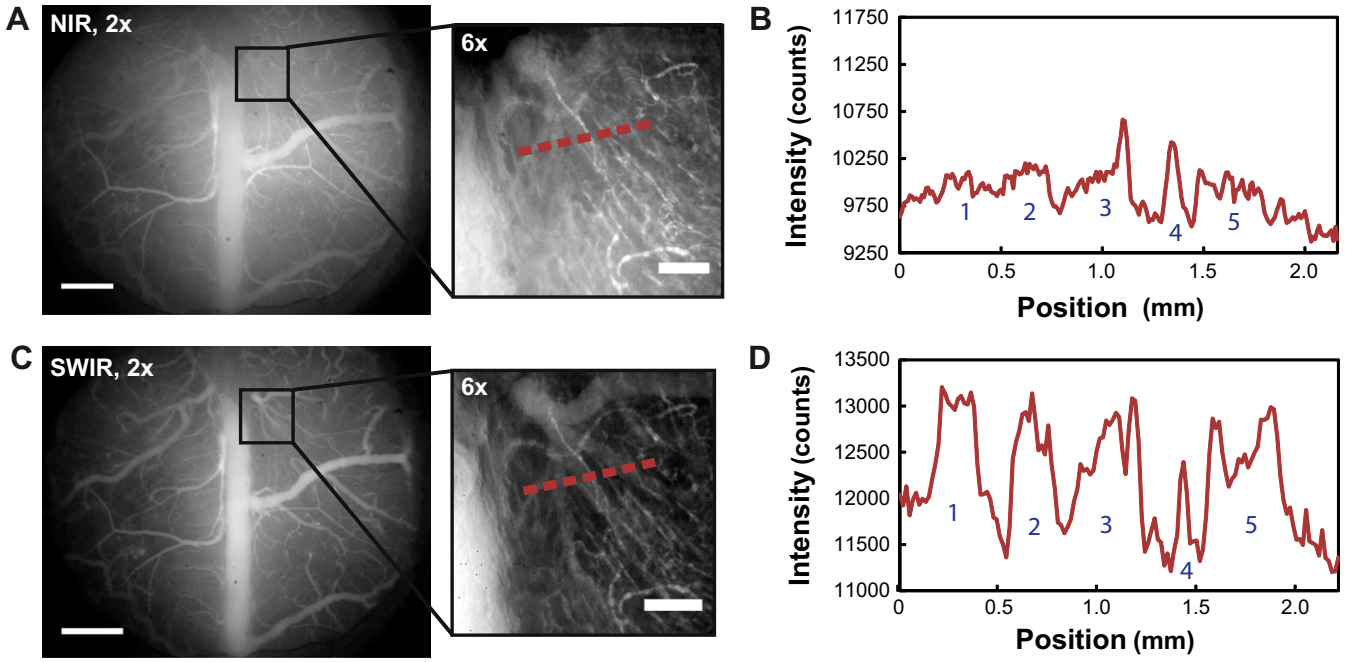

Fig. S4. High-contrast SWIR intravital microscopy of mouse brain vasculature. An aqueous ICG phospholipid mixture was injected via the tail vein of a mouse, and the fluorescence in the brain vasculature was imaged through a cranial window. (*A*) Microscopy of the brain vasculature through the cranial window shows poor contrast with 850-nm long-pass NIR detection. (*B*) The intensity across a line of interest (red line) shows insufficient contrast to resolve overlapping vessels from background signal. (*C*) Using 1,300-nm long-pass SWIR detection greatly improves image contrast and (*D*) resolution of the vessels. (Scale bars: *A*, *Left* and *C*, *Left*, 1 mm; *A*, *Right* and *C*, *Right*, 100 μm.)

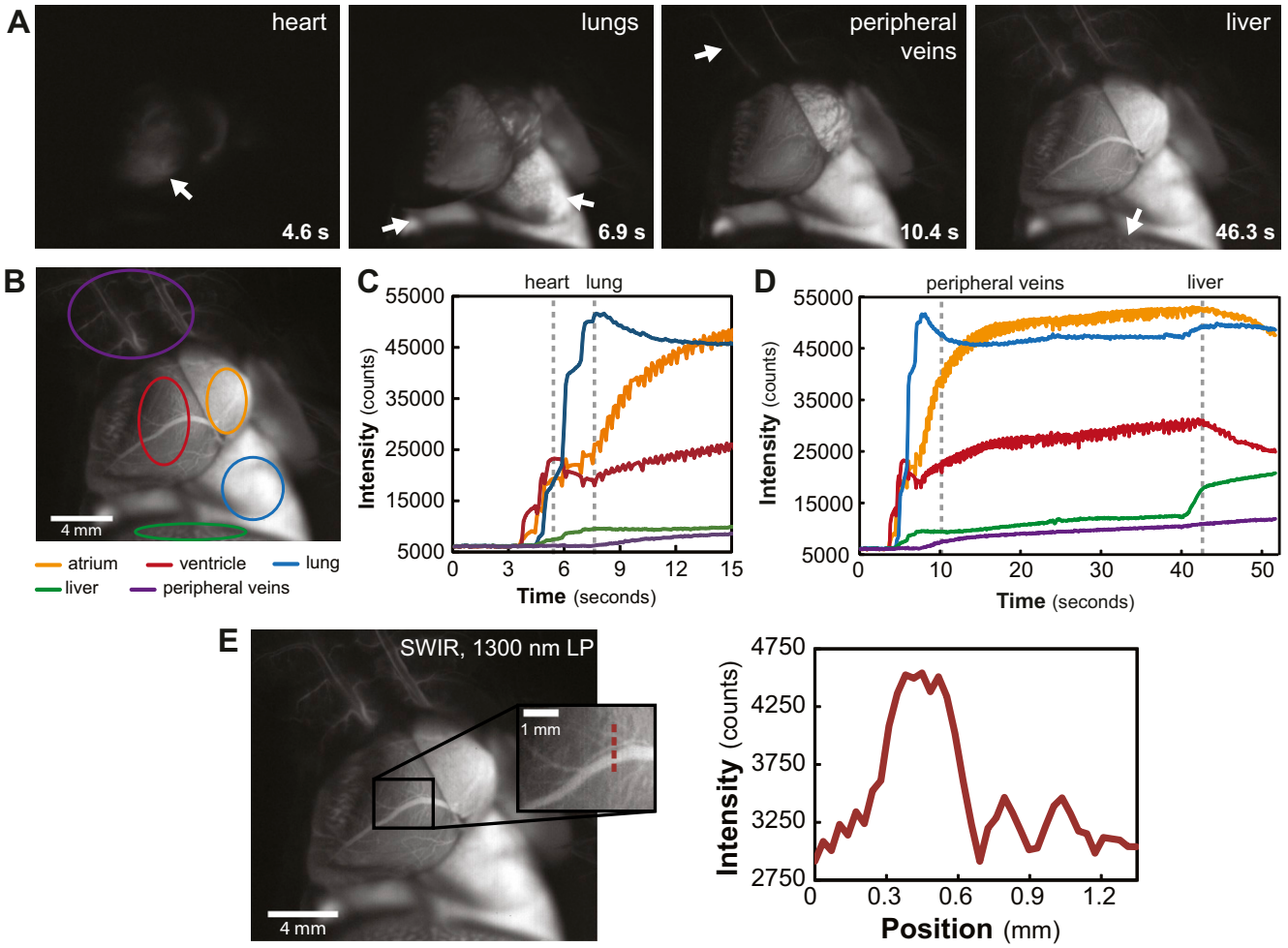

Fig. S5. Temporal and spatial resolution in intravital ICG angiography. SWIR fluorescence angiography was performed intravitally in three mice at 9.17 frames per second using ICG for contrast, diffuse 808-nm excitation, and a 1,300-nm long-pass emission filter on an InGaAs SWIR camera (Movie S2). (*A*) The heart of the mouse was exposed via surgery (1), and 200 μL of aqueous ICG (0.25 mg/mL) injected into the mouse via the tail vein was tracked as fluorescence first appears in the heart followed by the lungs, the peripheral veins, and finally, the liver. (*B*) The fluorescence intensities of the heart atrium (orange), heart ventricle (red), lung (blue), liver (green), and peripheral vasculature (purple) are plotted to show a single injection in one representative mouse as it (*C*) arrives first at the heart and the lungs and (*D*) at the peripheral vasculature before beginning to be cleared through the liver, which is known to be the main metabolic clearance site for ICG (2, 3). Images in *A* have the same scale as in *B*. (*E*) High spatial resolution was shown by measuring fine vasculature on the heart on the order of 100 μm in diameter.

1. Gage GJ, Kipke DR, Shain W (2012) Whole animal perfusion fixation for rodents. *J Vis Exp*, 10.3791/3564.
2. Leevy CM, Smith F, Longueville J, Paumgartner G, Howard MM (1967) Indocyanine green clearance as a test for hepatic function. Evaluation by dichromatic ear densitometry. *JAMA* 200:236–240.
3. Alander JT, et al. (2012) A review of indocyanine green fluorescent imaging in surgery. *Int J Biomed Imaging* 2012:940585.

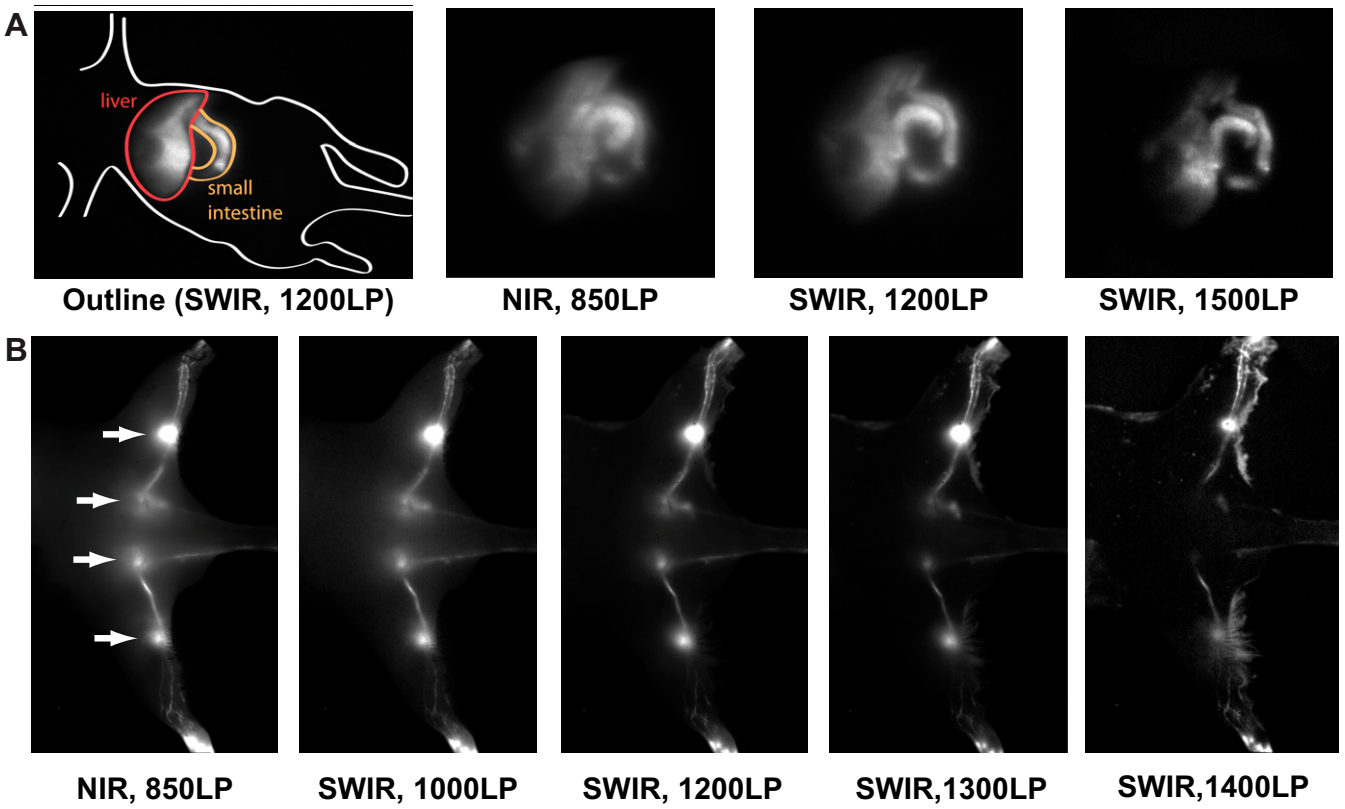

Fig. S6. Noninvasive imaging beyond 1,300 nm using ICG SWIR fluorescence. (*A*) Hepatobiliary clearance of ICG. Two hundred microliters of aqueous ICG (0.25 mg/mL) was injected into a mouse via the tail vein, and the liver and small intestine, outlined in red and yellow, respectively, were imaged noninvasively through the skin, shown here ~1.5–2 h after injection. The liver and small intestine were imaged in the NIR on a silicon camera with an 850-nm long-pass filter and in the SWIR on an InGaAs camera with a 1,200-nm long-pass filter and a 1,500-nm long-pass filter. The image acquired with the 1,500-nm long-pass filter shows a clear enhancement in image resolution. (*B*) Lymph node tagging. ICG (0.18 mg/mL) was injected s.c. into the hind feet and s.c. into the tail of a mouse, excited with 50–70 mW/cm^2 of 808-nm excitation light, and imaged noninvasively through the skin as it localized in the dorsal lymphatic vasculature and nodes (nodes are indicated with white arrows). The lymphatic system was imaged in the NIR with an 850-nm long-pass filter on a silicon camera and in the SWIR with 1,000-, 1,200-, 1,300-, and 1,400-nm long-pass filters on an InGaAs camera. While image contrast improves at longer wavelengths, deep lymph node signal is attenuated.

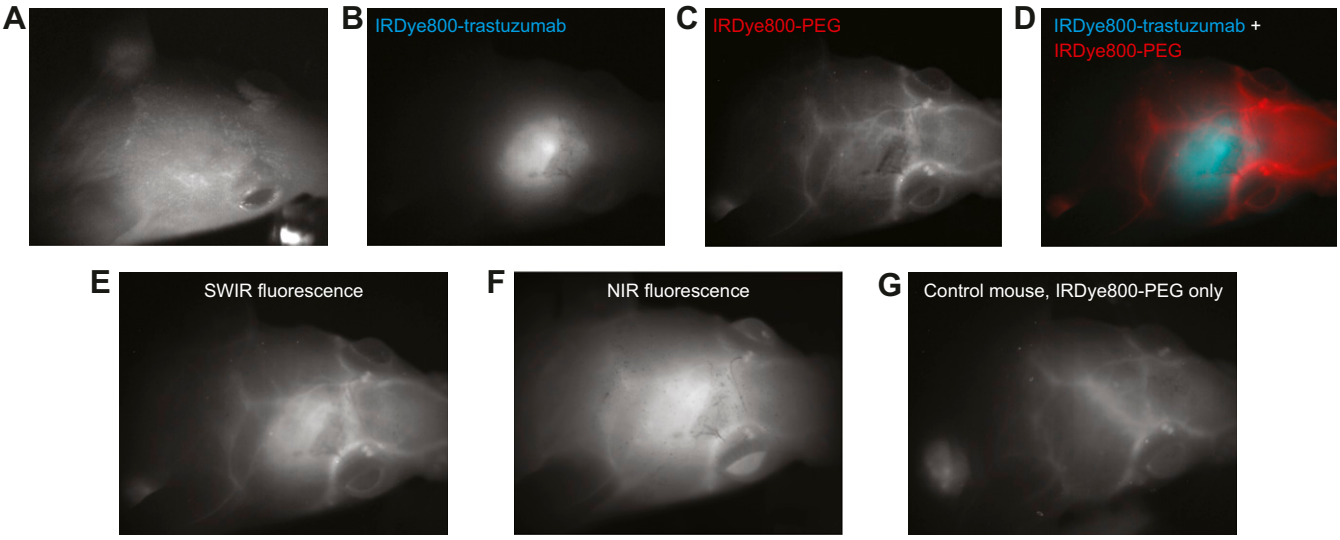

Fig. S7. Targeted SWIR imaging in vivo with IRDye 800CW. (*A*) A nude mouse with a brain tumor (~50–70 mm^3) from implanted human BT474 breast cancer cells is imaged here under room light illumination (bright-field imaging). (*B*) Three days after injecting IRDye 800CW–trastuzumab conjugate (15-mg/kg dose), fluorescence from the labeled tumor was imaged noninvasively through skin and skull on an SWIR camera with 1,150-nm long-pass emission detection. (*C*) Immediately, subsequent injection (up to 3 nmol) of IRDye 800CW conjugated to PEG was used to provide contrast to surrounding brain vasculature, which was temporally separated from the labeled tumor in postprocessing. (*D*) The tumor and vessel images were then assigned a color (blue and red, respectively) and overlaid to generate a false color fluorescence image of the tumor and its surrounding vasculature. The vessels overlaying the tumor are better defined using (*E*) SWIR imaging on an InGaAs camera with a 1,150-nm long-pass filter compared with (*F*) NIR imaging on a silicon camera with an 800-nm long-pass filter. (*G*) We also show a control mouse, which was implanted with a tumor and labeled with IRDye800 PEG but not labeled with IRDye800–trastuzumab, imaged with 1,150-nm long-pass detection on the SWIR camera.

Table S1. Details of the camera, emission filters, and exposure times used for each of the images and videos presented

Figure or movie	Camera	Filters	Exposure time, ms
Fig. 1*B*, *Inset*	NIRvana	2× FGL850S, liquid crystal bandpass filter	10,000
Fig. 2*E*	NIRvana	2× FGL1000S, FELH1300	1,000
Fig. 3 *A* and *C*	PIXIS	FELH0850	5
Fig. 3 *B* and *E*	NIRvana	FELH0850, FEL1000, FEL1300	5,000
Fig. 4 *A* and *B*	NIRvana	FELH1000, FELH1300	100
Fig. S2*A*	NIRvana	2× FGL1000S, FELH1300	1,000
Fig. S2 *C* and *D*	NIRvana	2× FGL1000S	1
Fig. S3*A*, columns 1 and 2	PIXIS	2× FGL850S, FELH0850	25
Fig. S3*A*, column 3	NIRvana	2× FGL1000S, FEL1000	500
Fig. S3*A*, column 4	NIRvana	2× FGL1000S, FELH1300	10,000
Fig. S3*B*	PIXIS	FELH0850	20
Fig. S3*C*	NIRvana	FELH0850, FEL1000, FEL1300	500
Fig. S3 *D*, *Upper Left* and *E*, *Upper Left*	PIXIS	FELH0850	5
Fig. S3 *D*, *Upper Right* and *E*, *Upper Right*	NIRvana	FELH0850, FEL1000, FEL1300	5,000
Fig. S3*D*, *Lower Left*	PIXIS	FELH0850	10
Fig. S3*D*, *Lower Right*	NIRvana	FELH0850, FEL1000, FEL1300	5,000
Fig. S4*A*, 2×	PIXIS	DMLP900, FELH0850	50
Fig. S4*A*, 6×	PIXIS	DMLP900, FELH0850	100
Fig. S4*C*, 2× and 6×	NIRvana	DMLP900, FELH1300	5,000
Fig. S5 *A*, *B*, and *E*	NIRvana	FELH1000, FELH1300	100
Fig. S5*A*, column 1	NIRvana	FELH0850, FELH1000, FELH1200	50
Fig. S5*A*, column 2	PIXIS	FELH0850	100
Fig. S5*A*, column 3	NIRvana	FELH0850, FELH1000, FELH1200	50
Fig. S5*A*, column 4	NIRvana	FELH0850, FELH1000, FEL1500	500
Fig. S5*B*, column 1	PIXIS	2× FGL 850S, FELH0850	10
Fig. S5*B*, column 2	NIRvana	2× FGL1000S, FELH1000	100
Fig. S5*B*, column 3	NIRvana	2× FGL1000S, FEL1200	1,000
Fig. S5*B*, column 4	NIRvana	2× FGL1000S, FEL1300	10,000
Fig. S5*B*, column 5	NIRvana	FELH1000, FEL1400	10,000
Fig. S7 *A* and *B*	NIRvana	FELH0850, FEL1000	500
Fig. S7 *C*–*E* and *G*	NIRvana	FELH0850, FELH1150	10,000
Fig. S7*F*	PIXIS	FELH0800	300
Movie S1	NIRvana	2× FGL1000S	1
Movie S2	NIRvana	FELH1000, FELH1300	100
Movie S3	NIRvana	FELH0850, FELH1000, FELH1200	50
Movies S4 and S5	NIRvana	2× FGL850S, FEL1000	100

The camera column refers to either the Princeton Instruments PIXIS-1024BR camera for NIR imaging or the Princeton Instruments NIRvana 640 for SWIR imaging. The filters column lists part numbers of the used Thorlabs filters. In general, the first letters of the part number indicate the filter type, and the following numbers indicate the respective wavelength. An S at the end of the nomenclature refers to a square filter, whereas the absence of an S denotes circular filters. DML, long-pass dichroic mirrors; FEL, long-pass edge-pass filters; FELH, premium hard-coated long-pass edge-pass filters; FGL, long-pass colored glass filters.

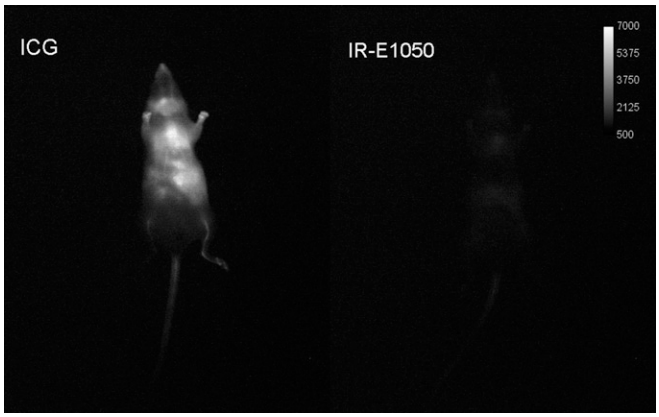

Movie S1. In vivo brightness comparison of ICG and IR-E1050. ICG and IR-E1050 were injected via the tail vein at the recommended doses (67 nmol for IR-E1050 and 64 nmol for ICG), excited with 808-nm excitation, and imaged noninvasively through the skin on an InGaAs SWIR camera using a 1,000-nm long-pass filter at 15 frames per second.

Movie S1

Movie S2. ICG SWIR intravital angiography in a mouse heart. Surgery was performed to open the chest of a mouse, exposing the heart, lungs, and liver for intravital imaging. Two hundred microliters of an aqueous ICG solution (0.25 mg/mL) was injected into the mouse via the tail vein, and the fluorescence was imaged using a 1,300-nm long-pass filter on an InGaAs SWIR camera, acquiring at 9.17 frames per second to image the fine vasculature on the surface of the heart while in motion.

Movie S2

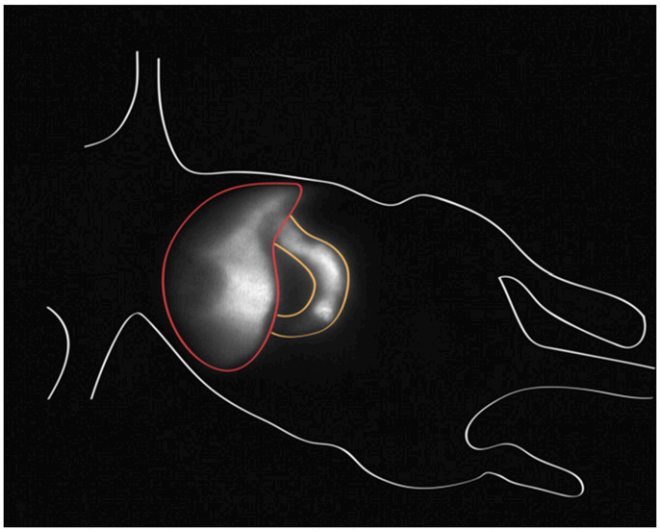

Movie S3. Noninvasive imaging of the hepatobiliary clearance of ICG. A mouse was injected with 200 μL of an aqueous ICG solution (0.25 mg/mL) via the tail vein. This video shows, ∼1 h after injection, the hepatobiliary clearance of ICG imaged noninvasively through the skin at 19.7 frames per second on an InGaAs camera with a 1,200-nm long-pass filter. The red outline indicates the position of the liver, which excretes the ICG into the small intestine (indicated by yellow outline). The imaging speed is sufficient to capture the peristaltic motions of the small intestine.

Movie S3

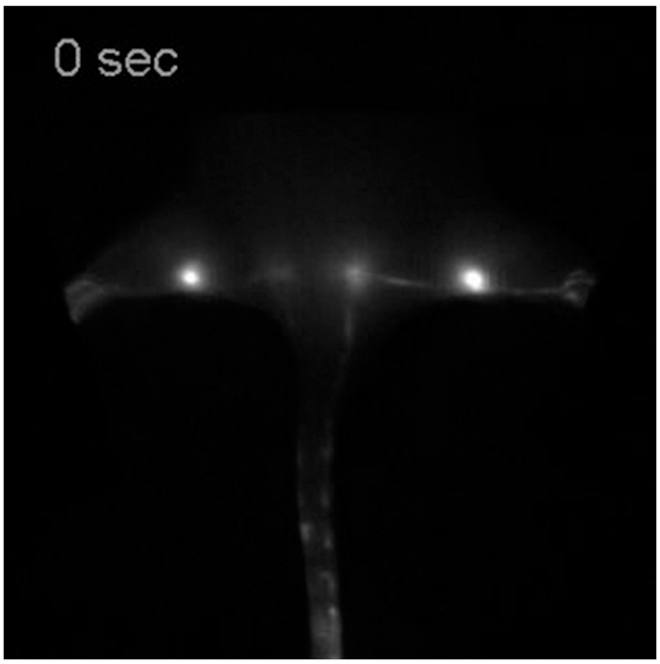

Movie S4. Real-time, noninvasive SWIR imaging of the lymphatic clearance of ICG. Aqueous ICG (0.18 mg/mL) was injected s.c. in the hind feet and s.c. in the tail of a mouse in 10–100 μL volumes. The lymphatic clearance of ICG by the dorsal lymph vessels and nodes is shown here imaged noninvasively through intact skin using 808-nm excitation light and an InGaAs SWIR camera with 1,000-nm long-pass detection and 9.17-frames per second acquisition.

Movie S4

Movie S5. Real-time, noninvasive SWIR imaging of the lymphatic clearance of ICG magnified. ICG (0.18 mg/mL) was injected s.c. in the hind feet and s.c. in the tail of a mouse in 10–100 μL volumes. The lymphatic clearance of ICG by the dorsal lymph vessels and nodes is shown here imaged noninvasively through intact skin using 808-nm excitation light and an InGaAs SWIR camera with 1,000-nm long-pass detection and 9.17-frames per second acquisition.

Movie S5